Author(s): Erlend Moldrheim, Michael J. Hannon, Isabelle Meistermann, Alison Rodger and Einar Sletten

Article Title: Interaction between a DNA oligonucleotide and a dinuclear iron(II) supramolecular cylinder; an NMR and molecular dynamics study

Year of publication: 2002

Link to published article: http;//dx.doi.org/10.1007/s00775-002-0354-2

Title page

Interaction between a DNA oligonucleotide and dinuclear iron(II) supramolecular cylinder; A NMR and molecular dynamics study.

Erlend Moldrheim · Einar Sletten ✉

Department of Chemistry, University of Bergen, Allegt. 41, N-5007 Bergen, Norway.

E-mail: *Einar.Sletten@kj.uib.no*

Phone: +47-55583352

Fax: +47-55589490

Michael J. Hannon · Isabelle Meistermann · Alison Rodger

Department of Chemistry, University of Warwick, Coventry, CV4 7AL, UK.

Keywords: Metallo-supramolecular · DNA oligonucleotide · NMR · Docking · Molecular Dynamics

Abbreviations: NOESY Nuclear Overhauser Enhancement SpectroscopY · TOCSY Total Correlation SpectroscopY · ROESY Rotating frame Overhauser Enhancement SpectroscopY · ESP ElectroStatic Potential · CHELPG CHarges from ELectrostatic Potentials-Grid based · PME Particle Mesh Ewald · MD Molecular Dynamics · VMD Visual Molecular Dynamics

Interaction between a DNA oligonucleotide and dinuclear iron(II) supramolecular cylinder; A NMR and molecular dynamics study.

Erlend Moldrheim · Michael J. Hannon · Isabelle Meistermann · Alison Rodger · Einar Sletten

Abstract

A tetracationic supramolecular cylinder, $[Fe_2L_3]^{4+}$ ($L=C_{25}H_{20}N_4$), with a triple-helical architecture is just the right size to fit into the major groove of DNA and too big to fit into the minor groove [*Angew. Chem. Int. Ed*. 2001, **40**, 879-884]. A detailed NMR spectroscopic analysis supported by molecular dynamics calculations shows unambiguously the close fit between the cylinder and a duplex oligonucleotide, $[d(GACGGCCGTC)_2]$. Furthermore, only the left-handed enantiomer of the cylinder seems to fit the groove geometry. With both free and complexed species of $[Fe_2L_3]^{4+}$ and DNA in solution the NMR spectra are too complicated for a detailed structure determination. Based on differences in chemical shifts and extensive Molecular Dynamic (MD) calculations a realistic qualitative picture of the DNA-cylinder adduct are presented. Several sets of chemical shifts assigned to the protons of the three ligand strands in the cylinder indicate that the iron complex situated in the major groove exhibits restricted rotation on the NMR time scale around the cylindrical axis. The NMR NOE data support a model where the cylinder undergoes both a translational and rotational oscillation in the major groove. The results of NOE restrained MD calculation indicates that the cylinder induces a 40^o degree bend of the double helix in accordance with linear dichroism (LD) measurements. Other distinct features to be noticed are the very low value of the helical twist (16^o) induced at the central G_4C_5 step.

Introduction

While DNA encodes the essential blueprint for life, within biological systems its structure and function are regulated by proteins. These proteins generally achieve sequence specific code recognition through surface motifs which interact with either the minor or, more commonly, the major groove of DNA in a non-covalent fashion. In the post genomic environment the ability to artificially stimulate or prevent the processing of the genetic code is an important goal and offers new opportunities for disease prevention or control. To achieve this, synthetic agents are required that recognise the genetic code in a sequence selective fashion: Synthetic agents that target the major groove of DNA with recognition through non-covalent surface motifs therefore have the potential to be a powerful new tool. However, to date little progress has been made in this direction, due in large part to the size of the molecular surfaces required to achieve this. Indeed synthetic molecules that do achieve sequence selectivity, such as amide linked imidazole/ pyrrole oligomers which bind in the minor groove [2], are rare. Oligonucleotides (synthetic and natural) can selectively recognize DNA by forming triplexes through binding in the major groove [3] and neutral oligonucleotide analogues (*e.g.* PNAs) can achieve similar effects, although more commonly they achieve sequence selectivity through strand displacement [4].

Metal complexes are particularly attractive vectors for non-covalent DNA recognition because of the cationic charge that the metallo-centres can impart which affords a substantial energetic contribution to the non-covalent binding to anionic DNA. Covalent DNA binding by metal complexes (*e.g.* cisplatin) has been extensively studied and usually focuses on binding to N7 of G and A residues [5]. Non-covalent binding of metal complexes to DNA is a less well developed area and

has primarily centered around spherical ruthenium polypyridyl complexes and complexes bearing planar intercalating units (or combinations thereof) [6-8]. Their small size often results in their location in the minor rather than the major groove and also means that they cannot target more than 2 base pairs. Consequently they do not afford surfaces best suited to act as scaffolds for sequence specific recognition. Supramolecular chemistry provides methodology for the design of large synthetic arrays and consequently allows us synthetically to bridge the size-gap between traditional small molecule and larger biomolecule DNA recognition-motifs. In particular, we have developed an "inexpensive approach" to generate sophisticated supramolecular architectures based on the interaction of metal ions with imine-based ligands [9-12]. Of particular importance to this work, a synthetic procedure has been described for making a tetracationic supramolecular cylinders with a triple helical architecture (Fig. 1) which are just the right size to fit into the major groove of DNA and too big to fit into the minor groove [1,12,13]. We describe herein the binding of such a supramolecular metallo-cylinder to a DNA oligonucleotide. A preliminary report on this work has recently been published [1]. The present paper describes in detail the results of NMR spectroscopic work and molecular dynamics calculations for the DNA-cylinder system.

Insert Fig. 1.

Materials and methods

The synthesis of $[Fe_2L_3]Cl_4$ (L= $C_{25}H_{20}N_4$) (Fig. 1) has been described previously [12, 13]. The sodium salt of the deoxyoligonucleotid, $[d(G_1A_2C_3G_4G_5C_6C_7G_8T_9C_{10})_2]$, was purchased from Oswel DNA Service and purified with ion-exchange

chromatography, desalted and paramagnetic impurities were removed using a Chelex 100 column (Sigma-Aldrich). The oligonucleotide was then dissolved in 90 % H_2O and 10 % D_2O containing 50 mM phosphate buffer and 40 mM NaCl, final concentration 2.8 mM in duplex. Aliquots of $[Fe_2L_3]Cl_4$ were added in five steps the duplex sample to reach a 1:2 ratio. This ratio was selected so that no precipitation should occur. NMR spectra were recorded on a Bruker DRX 600 MHz instrument. A combination of through- space nuclear Overhauser effect (NOESY) and through-bond correlated (TOCSY) two-dimensional spectra were recorded at 17 °C using Double Pulsed Field Gradients Spin Echo water suppression (dpfgsew5) [14, 15]. The data were processed using XWIN-NMR (Bruker) and analyzed using Sparky [16]. All five imino protons involved in Watson-Crick hydrogen bonding were clearly observed in the 1D spectrum for the free duplex. The assignments for the imino resonances in the adduct were obtained from a NOESY spectrum (Fig. S1).

Based on the fact that the interaction between $[Fe_2L_3]^{4+}$ and DNA is expected to be purely electrostatic we decided to investigate this using molecular docking calculations using the DOCK 4.0.1 suite of programs (University of California, San Francisco) [17]. The duplex geometry of the oligonucleotide was built using standard B-DNA parameters in InsightII (Biosym ltd.). Based on NOESY cross peaks between the cylinder and the duplex, a selected clusters was generated in the major groove. A box with dimensions 14.2 x 14.1 x 14.1 (Å) was constructed around these clusters and a grid calculation were carried out with the grid spacing 0.15 Å. Initially the docking was performed with a sampling size of 10000 structures. The 15 best results were then energy minimized using a more conservative convergence criterion than suggested in the DOCK manual.

To be able to describe the interaction between the cylinder and DNA in more detail, we needed to investigate the possibility for the cylinder to induce conformational changes in the nucleic acid. Docking simulations are able to include flexibility for the ligands, but not for the receptor. In our case a reasonable assumption is that the cylinder maintains its geometry with small or no alterations at all, while the nucleic acid, which is relatively flexible are able to adopt various conformations depending on the surrounding environment. The most adequate method to investigate conformational changes of nucleic acids is molecular dynamics simulations in explicit solvent [18].

Development of parameters for the cylinder was essential for a molecular dynamics study on the interaction between $[Fe_2L_3]^{4+}$ and [d(GACGGCCGTC)$_2$]. As the size of $[Fe_2L_3]^{4+}$ would demand extensive computational power to perform a complete *ab intio* study, a geometry optimization was carried out starting from the X-ray structure of $[Fe_2L_3]^{4+}$ [19] using the semi-empirical PM3(tm) method included in Titan software [20, 21]. Due to the two-fold symmetry of the cylinder, we reduced the number of atoms prior to the *ab initio* calculation by removing the phenylene-methylene bonds and replacing them with hydrogen atoms. Without further geometry optimization these coordinates (now $[Fe(C_{12}H_{10}N_2)_3]^{2+}$) were used as input structure in a single point calculation using the quantum chemistry software Gaussian98 [22]. Density functional calculations were performed at the B3LYP level of theory where molecular orbitals were formed in atomic-orbital basis 6-31G(d) [23].

The Merz-Kollman scheme was first applied [24, 25] to calculate the electrostatic potential (ESP) charges. To our surprise this method led to negative charges on iron(II) and positive charges on the nitrogens. As these charges appeared unrealistic we decided to calculate the charges using the CHELPG [26] method,

creating an electrostatic potential grid suitable as input for RESP [27] (restrained electrostatic potential fitting program in Amber 6.0). By careful examination of the result we found that RESP did not alter the charges significantly. With this result in mind the ESP grid was recalculated with increased density of the grid points (Gaussian98 options 6/33= 2, 6/41= 10, 6/42= 2) and the resulting CHELPG charges applied directly (Fig. S1 and Table S1). Without having a realistic option to calculate a Hessian matrix and extract force constants for the cylinder from this, we had to rely on previously determined force constants for a system containing Fe(II)-N bonds. This approach was considered to be appropriate as the geometry of $[Fe_2L_3]^{4+}$ is expected to be quite rigid and consequently could be subjected to constraints (NTR constraints) during the simulation. As the basis for the determination of force constants for the iron(II) centers we used the porphyrin model present at the Amber web-site [28]. Force constants for the C-C and C-N bonds were determined using the mean bond lengths found for the respective bonds in $[Fe_2L_3]^{4+}$ and interpolating between the force constants for pure single and pure double bonds. The other parameters were determined comparing atom types present in the Parm99 force field recently published by Wang et al. [29] and atom types defined for the cylinder. The parameters were included using the XLeap module of the Amber 6.0 software suite, adding four chlorine ions to neutralize the charge of +4.

All of the subsequent calculations were carried out using the Amber 6.0 software suite [30]. The nucleic acid was built using Nucgen with standard B-DNA parameters. The DNA was then loaded into XLeap using the Parm99 force field and neutralized by adding 18 Na^+ as counter-ions. $[Fe_2L_3]^{4+}$ was docked manually into the major groove of $[d(GACGGCCGTC)_2]$ according to the position indicated from both NMR and docking results [1]. The DNA-cylinder adduct was then surrounded by a

periodic box of water described by the TIP3P potential [31] extended to 9 Å from any solute atom, containing 5434 water molecules in total. Equilibration of the system was carried out using the Sander program with SHAKE [32] on the hydrogen atoms with a tolerance of 0.0005 Å and a 2 fs time step. A 9 Å cutoff to the Lennard-Jones interactions was applied. After 500 steps of energy minimization a 100 ps molecular dynamics simulation were performed heating the system from 100 K to 300 K over a time period of 10 ps. Subsequently the temperature was reduced to 300 K for the remaining 90 ps using the Berendsen temperature coupling algorithm [33] with a time constant of 0.2 ps. The particle mesh Ewald method (PME) [18, 34, 35] with a charge grid spacing of approximately 1.0 Å was used, interpolating the grid using a cubic b-spline with the direct sum tolerance of 10^{-6} at the 9 Å direct space cutoff. The atomic positions of the DNA and the cylinder were fixed. Subsequently, 1000 steps of minimization with 25 kcal/(mol·Å^2) restraints on the DNA were carried out, followed by a 3 ps MD simulation using the same restraints. The 500 kcal/(mol·Å^2) restraints on $[Fe_2L_3]^{4+}$ were kept throughout the equilibration. The equilibration was continued with five rounds of 1000 steps energy minimizations where the DNA restraints were reduced by 5 kcal/(mol·Å^2) for each run. The final equilibration was carried out with 100 ps of MD where the system was heated from 100 K to 300 K during the first 10 ps. followed by a 1.0 ns MD simulation on the free oligonucleotide using the resulting structure as the starting structure for the $[d(GACGGCCGTC)_2]$/ $[Fe_2L_3]^{4+}$ system. For this system we performed a 1.5 ns simulation where the positional restraints of 500 kcal/(mol·Å^2) for the cylinder were maintained throughout the trajectory. The trajectories were analyzed using the trajectory analyzing modules PTRAJ and CARNAL of Amber 6.0. Visual inspections of the trajectories were performed using VMD [36]. Average structures from the trajectories were calculated using the PTRAJ

module [30] and no extra processing of the averaged coordinates were performed. The calculations were performed either on a Linux workstation or on a SGI Cray Origin 2000 supercomputer at the University of Bergen. Helical parameters were generated with the program 3DNA [37] and Curves 5.3 [38].

Results and discussion

NMR results

$[Fe_2L_3]^{4+}$ is very soluble in aqueous solution, but due to the high positive charge and the relatively short oligonucleotide used in this study, we observed precipitation beyond a $[Fe_2L_3]^{4+}$/ DNA ratio of 1:2. Evidently this precipitation is caused by charge neutralization, which has been observed with ditercalinium (a positively charged bisintercalating molecule) complexed to short oligonucleotides [39] and also with binding of simple divalent metal ions (*e.g.* Hg^{2+}) to duplexes [40]. The step-wise addition of $[Fe_2L_3]^{4+}$ to the duplex solution to reach the 1:2 ratio were followed by 1D ^{1}H NMR. The color of the solution was now deep purple (the color of the cylinder) and there was no sign of precipitation over a period of several months. The base pairing of the oligonucleotide was maintained as confirmed by the presence of Watson-Crick imino protons both in the free and complexed form of the duplex (Fig. 2 and Table 1, Fig. S2). It should be noted that several attempts were made to prepare samples with higher concentrations of the cylinder involving extensive stirring, the use of various co-solvents and different salt concentrations. However, these attempts were not successful.

Insert Fig. 2 and Table 1.

Since the solution contains both free and complexed DNA the resulting NMR spectra are quite complex and difficult to analyze. Still we were able to assign the majority of the signals belonging to both the free and bound DNA. The 2-fold symmetry of the central part of the palindrome is lifted upon coordination with $[Fe_2L_3]^{4+}$. This is clearly seen in the TOCSY spectrum (Fig. 3), where the number of cross-peaks originating from the coupling between H5 and H6 on the cytosines C3, C6 and C7 increased from three to six (C3II is overlapped with C3). Thus, we were able to assign a double set of nucleotide resonances, which are labeled I and II. This change in symmetry has also been observed for other groove binding and intercalating molecules [41- 43]. The fact that relatively narrow linewidths are observed for the resonances of the DNA-cylinder indicates that this adduct is quite stable. This is in agreement with an ethidium bromide (EB) fluorescence competition binding assay previously performed by Rodger et al. [13], showing that $[Fe_2L_3]^{4+}$ has a binding constant towards DNA that is higher than EB (in the order 10^7 M^{-1}).

Insert Fig. 3 and Fig. 4.

Variations in chemical shift between free and bound DNA (Table 1 and Fig. 4) indicate significant conformational changes in $[d(GACGGCCGTC)_2]$ upon complexation with the cylinder. The largest changes in chemical shift are found in the central G-G-C-C quartet. As the interaction between the cylinder and DNA is primarily electrostatic it is likely that the chemical shift effects found for the nucleotide protons are induced either by conformational changes to the DNA and/or influence by ring current effects generated by the proximity of the six phenyl groups

of the $[Fe_2L_3]^{4+}$ ligands. In a double helical environment the position of sugar proton resonances from H2' is mainly affected by the ring current and magnetic anisotropy of the base attached to this sugar [44]. Furthermore, it has been suggested that the H2' signal should be rather sensitive to deviations from regular double helical conformation [44-46]. For example, a large upfield shift of H2' in a cis-platinated duplex was attributed to shielding by the destacked adenine base of the kinked structure [46]. It is now well established that Y-R steps (Y= pyrimidine, R= purine) like CpG are geometrically flexible [47] and several studies have shown that CpG steps are involved in DNA bending [48, 49]. Since linear dichroism shows that very low loading of $[Fe_2L_3]^{4+}$ have a dramatic bending effect on the DNA [1] and atomic force microscopy images show that this is an intramolecular effect resulting in coils of DNA [1] it is interesting to look for similar bending pattern in the NMR data. The H2' resonances of the central residues G5II and C6I of the adduct display significant upfield shifts in accordance with a bent structure found by other methods (*vide supra*). However, similar upfield shifts are also observed for the corresponding H2'' resonances. Thus, the proximity of the cylinder ligand containing six ring-current producing phenyl groups which prevents a quantitative conformational analysis based on chemical shifts.

Insert Fig. 5.

The sequential walk between base protons and the H1' protons are shown in Fig. 5 for the free duplex and for the two strands I and II in the adduct. Every expected crosspeak is present (though partially overlapped), but the intensity of the

crosspeaks in the central region is decreased. This is most noticeable for the crosspeaks G5I H1' to C6I H5 and C6II H1' to C7II H6.

The chemical shift data and intra-molecular NOE's originating from $[Fe_2L_3]^{4+}$ are presented in Table 2 and 3, respectively. Five different sets of signals (S1-S5) were observed for the cylinder. Based on ROESY data from the free cylinder we were able to assign the ^1H shift with respect to their position in the ligands. It should be noted that the set S5 has a noticeable lower intensity than the sets S1-S4. However, due to the equivalence of the ligand strands and the presence of slow exchange, we were not able to determine from which of the three ligands strands the different sets were originating. These sets displayed minor variations of the intensities in the NOESY spectra of the system, but the chemical shifts from the different sets of the cylinder protons were with a few exceptions overlapped with either cylinder protons or DNA protons.

Insert Table 2 and 3.

The NOE contacts (Table 3) between the $[Fe_2L_3]^{4+}$ and $[d(GACGGCCGTC)_2]$ show that the cylinder is situated in the major groove. However, several possibilities exist as to the nature of the DNA- cylinder interactions. One may envisage a system where iron complex exhibits fast rotation on the NMR time scale around the cylindrical axis. In this case at most two sets of proton resonances from the cylinder should be observed. At the other extreme, the cylinder might be fixed in one position in the groove, giving rise to six sets of proton resonances. A more plausible situation would be a restricted helical oscillating motion in the major groove involving both

rotation and translation. This latter model is supported by the fact that two sets of chemical shifts, S1/ S2 and S3/ S4, and the corresponding NOE contacts are located toward strand I and II, respectively. The assignments do not specifically lock one proton on the cylinder to one specific ligand strand (L1, L2 or L3) thus, it is expected that rotation of $[Fe_2L_3]^{4+}$ will bring this proton into the proximity of close-by DNA protons. Introducing functional groups on $[Fe_2L_3]^{4+}$ which *e.g.* could facilitate hydrogen bonding to the DNA bases, would allow the cylinder to be locked in one position in the groove.

Docking results

The binuclear iron(II) cylinder is an enantiomeric molecule and both forms are present in the solution. Recently we were able to separate the two enantiomers [50] and tests against DNA using linear dichroism [LD] show that left handed enantiomer displays the highest activity towards DNA. By utilizing simple molecular modeling the left handed enantiomer was found to fit the major groove of a right handed B-DNA much better than the right handed form. To further test whether the major groove of DNA is a likely coordination site for $[Fe_2L_3]^{4+}$ or not, we performed molecular docking calculations using DOCK 4.0 [17]. At this stage the canonical B-DNA version of $[d(GACGGCCGTC)_2]$ as the receptor for the cylinder was used. The docking calculations were performed using two kinds of scoring functions; contact score (molecular shape complementarity) and energy score [51] (based on non-bonded terms of the Amber force field). Among the 15 top-scoring results with respect to contact score, ten complexes were almost superimposed in the middle of the major groove (spanning C3 to G8). The other five were spanning G4 to T9. The

results calculated with respect to energy score were not that homogeneous. Here only three out of fifteen complexes were located in the middle of the groove. The six top-scoring complexes were all located between G4 and T9. A closer inspection of the results showed that the intermolecular van der Waals energy was the dominating factor with respect to the energy score. The three complexes in the middle of the groove have all favorable values for the intermolecular electrostatic energy but correspondingly higher values for the intermolecular van der Waals energy. The left handed enantiomer of $[Fe_2L_3]^{4+}$ displays a remarkable fit in the groove where two of the pyridine rings of ligand strands L_1 and L_2 «follow» the base geometry of the two nucleotide strands (Fig. S3).

Molecular dynamics calculations, free DNA and DNA-cylinder adduct

Initially, MD calculations were carried out for the free DNA duplex in order to check any sequence-specific structural deviations from regular B-form DNA. The averaged structure from the last 200 ps of the 1.0 ns trajectory of the free duplex displays a number of interesting features (Fig. S4). The structure is characterized by a wide major groove in the central part and a moderate bend (10.3 degrees). Other features of the structure are negative x-displacement values for all base pair steps except at the ends and positive tip and roll values for the two CpG steps.

The parameters developed for $[Fe_2L_3]^{4+}$ were primarily prepared to account for the charge of the complex. Reasonable force constants were extracted by comparing the geometry for atom types included in the latest force field published for Amber [29] and with the atoms in $[Fe_2L_3]^{4+}$. The results of a relatively short MD test run (150 ps) showed that the coordination geometry around the two irons changed from the

pseudo-octahedral geometry found in the X-ray structure [19] to a geometry best described as a compressed octahedron. Since this result indicated that the parameters around iron(II) were not optimal, further MD calculations were carried out using positional restraints for the cylinder to maintain the X-ray structure during the simulation.

Insert Fig. 6.

Snapshots of the 1.5 ns trajectory from the molecular dynamics simulation performed on the $[Fe_2L_3]^{4+}$/[d(GACGGCCGTC)$_2$] system clearly shows that the cylinder has a dramatic influence on the conformation of the oligonucleotide (Fig. 6). A more detailed analysis of the simulation process is given in Fig.s 7-9. The most remarkable feature is the bending of DNA which was measured using the distance between the center of mass of the first base-pair and the center of mass of the last base-pair (Fig. 7). The bending reaches a maximum of 38.9 degrees at 496 ps, but decreases significantly over the next 150 ps. During the following ~700 ps the DNA displays a distinct stretched structure (Fig. 6). With no anchoring restraints imposed, the cylinder is seen to move away from the initial coordination site during the long trajectory. The animation of the trajectory using VMD shows that the cylinder moves down the major groove with one end aligning along the phosphate backbone and the other end facing out of the major groove during the last ~200 ps. The variation in rms deviation during the simulation run (Fig. 8) was calculated with the equilibrated structure as a reference and follows the change in curvature, which apparently is the major contributor to the rms deviation.

Insert Fig. 7-9.

NOE restrained MD calculations

Based on NOESY data alone it was not possible to carry out a complete NMR structure determination of the DNA-cylinder adduct due to excessive overlap in the 2D spectra. An alternative approach was to use inter-molecular NOE contacts as anchors in a molecular dynamics simulation. To test this possibility we used a few unambiguous NOE contacts as anchors in an explicit water MD simulation. The same protocol for equilibration as previously described was used, except that the number of minimization steps was increased from 1000 to 2000. The system was let to equilibrate over a period of 50 ps. In this period the system was heated from 100 K to 380 K over a period of 5 ps and then cooled slowly to 300 K over a period of 5 ps. In the remaining 40 ps the system was equilibrated to constant temperature (300 K). During this simulation the system appeared to reach an equilibrated state. A relatively short production run of 400 ps was then performed. The entire system and a close-up of the central part of the adduct based on coordinates averaged over 200-400 ps from the restrained MD calculations are shown in Fig. 10 and 11. A comparison of these coordinates and the coordinates from the 1.5 ns trajectory is shown in Fig. 12.

Insert Fig. 10-12.

Helical parameters

The helical parameters given in Fig. 13 are calculated for the DNA adduct, free DNA and canonical B-form DNA. The coordinates for free DNA are those based on the averaged structures over the last 200 ps from the 1.0 ns trajectory, whereas the averaged structure for the DNA adduct was calculated using the coordinates from 1360-1500 ps. The results show several structural changes, particularly in the central part of [d(GACGGCCGTC)$_2$] where the $[Fe_2L_3]^{4+}$ induces a noticeable shift of symmetry in the duplex. Thus, the MD simulation supports the lift of symmetry found in the NMR spectra of the system. The wide major groove found in the free DNA is extended even more to accommodate the cylinder (Fig. 14). Among other distinct features of the structure, which differ from the free DNA is the low value for the helical twist (16.05 degrees) found for the G_4pG_5 step. This step also displays a low value for the y-displacement, a high value for the inclination and a very small rise. The G_5pC_6 step follows the base pair step parameters of canonical B-DNA with surprising accuracy, but clearly deviates with the results found for the free DNA. Furthermore, the parameters of the G_5-C_{16} and C_6-G_{15} base pairs exhibit distinct differences for stretch, buckle and propeller twist. The C_6pC_7 step is characterized by a large value for the rise parameter where the distance between the base pairs is 3.77 Å. During parts of the trajectory one of the pyridine rings on $[Fe_2L_3]^{4+}$ is partially intercalated between C6 and C7. NMR data were not able to confirm this mode of interaction. High values for inclination and rise characterize the C_7pG_8 step.

Insert Fig. 13 and 14.

Conclusion

We have presented a detailed analysis of the interaction between a binuclear iron(II) supramolecular cylinder and the DNA decamer [d(GACGGCCGTC)$_2$] with the use of NMR, molecular docking and molecular dynamics calculations, which reveal the potential of this cylinder to act as a major groove binder. The interaction mode of the cylinder is characterized by its ability to induce conformational changes in DNA. This has been shown by a combination of NMR spectroscopy and molecular dynamics calculations. The development of synthetic major groove binding agents, which recognize the DNA through non-covalent interactions inducing dramatic structural effects, has important implications for genome recognition and we are currently extending our studies to functionalized systems and enantiopure cylinders. Based on the present results one way to proceed is to attach polar groups to the cylinder to act as either hydrogen bond donors or acceptors in the major groove involving base nitrogen atoms and /or carbonyl groups. In this way the cylinder could be locked to dsDNA in a sequence-specific manner depending on the position of the polar groups.

Acknowledgments: This work was supported by The Norwegian Research Council (135055/410), the Leverhulme Trust (F/215/BC) and the EPSRC lifesiences network (GR/M91105) and the University of Warwick. Dr. Knut Børve (Department of Chemistry, University of Bergen) and Dr. Ulf Ryde (Department of Theoretical Chemistry, University of Lund, Sweden) have been of great help in the preparation of force field parameters for $[Fe_2L_3]^{4+}$. Computer time from Parallab High Performance Computer Center at the University of Bergen is gratefully acknowledged.

References

1. Hannon MJ, Moreno V, Prieto MJ, Moldrheim E, Sletten E, Meistermann I, Isaac CJ, Sanders KJ, Rodger A (2001) Angew Chem Int Ed 40: 879-884
2. White S, Szewczyk JW, Turner JM, Baird EE, Dervan PB (1998) Nature 391: 468-471
3. Thuong NT, Helene C (1993) Angew Chem Int Ed 32: 666-690
4. Nielsen PE, Haaima G (1997) Chem Soc Rev 26: 73-78
5. Lippert B (ed) (1999) Cis-platin, a leading anti-cancer drug VCH, Weinheim
6. Coggan DZM, Haworth IS, Bates PJ, Robinson A, Rodger A (1999 Inorg Chem 38**:** 4486-4497
7. Onfelt B, Lincoln P, Norden B (1999) J Am Chem Soc 121: 10846-10847
8. Erkkila KE, Odom DT, Barton JK (1999) Chem Rev 99: 2777-2795 and refs therein
9. Childs LZ, Alcock NW, Hannon MJ (2001)Angew Chem Int Ed 40: 1079-1081
10. Hannon MJ, Painting CL, Alcock NW (1999) Chem Commun 2023-2024
11. Hannon MJ, Bunce S, Clarke AJ, Alcock NW (1999) Angew Chem Int Ed 38: 1277-1278
12. Hannon MJ, Painting CL, Jackson A, Hamblin J, Errington W (1997) Chem Commun 1807-1808
13. Rodger A, Sanders KJ, Hannon MJ, Meistermann I, Parkinson A, Vidler DS, Haworth IS (2000) Chirality 12: 221-236
14. Liu AM, Mao X, Ye C, Huang H, Nicholson JK, Lindon JC (1998) J Magn Res 132: 125-129
15. Hwang T-L, Shaka AJ (1995) J Magn Res Series A 112: 275-279
16. Goddard TD, Kneller DG, SPARKY3, University of California, San Francisco

17. Ewing TJA, Kuntz ID (1997) J Comp Chem 18: 9, 1175-1189
18. Cheatham III TE, Kollman PA (2000) Annu Rev Phys Chem 51: 435-471
19. Hannon MJ, Painting CL, Alcock NW, Childs LJ, Liu Z (manuscript in preparation)
20. Stewart JJP (1989) J Comp Chem 10: 209-220
21. Titan, Wavefunction, Inc, 18401 Von Karman Ave, Ste 370, Irvine, CA 92612 USA
22. Gaussian 98, Revision A9, Frisch MJ, Trucks GW, Schlegel HB, Scuseria GE, Robb MA, Cheeseman JR, Zakrzewski VG, Montgomery Jr JA, Stratmann RE, Burant JC, Dapprich S, Millam JM, Daniels AD, Kudin KN, Strain MC, Farkas O, Tomasi J, Barone V, Cossi M, Cammi R, Mennucci B, Pomelli C, Adamo C, Clifford S, Ochterski J, Petersson GA, Ayala PY, Cui Q, Morokuma K, Malick DK, Rabuck AD, Raghavachari K, Foresman JB, Cioslowski J, Ortiz JV, Baboul AG, Stefanov BB, Liu G, Liashenko A, Piskorz P, Komaromi I, Gomperts R, Martin RL, Fox DJ, Keith T, Al-Laham MA, Peng CY, Nanayakkara A, Challacombe M, Gill PMW, Johnson B, Chen W, Wong MW, Andres JL, Gonzalez C, Head-Gordon M, Replogle ES, Pople JA, Gaussian, Inc, Pittsburgh PA, 1998
23. Rassolov VA, Pople JA, Ratner MA, Windus TL (1998) J Chem Phys 109: 1223-1229
24. Singh UC, Kollman PA (1984) J Comp Chem 5: 129-145
25. Besler BH, Merz KM, Kollman PA (1990) J Comp Chem 11: 431-439
26. Breneman CM, Wiberg KB (1990) J Comp Chem 11: 361-373
27. Bayly CI, Cieplak P, Cornell WD, Kollman PA (1993) J Phys Chem 97: 10269-10280

28. http://www.amber.ucsf.edu/amber/ff94/contrib/heme/frcmodhemall

29. Wang J, Cieplak P, Kollman PA (2000) J Comp Chem 21: 1049-1074

30. Case DA, Pearlman DA, Caldwell JW, Cheatham III TE, Ross WS, Simmerling CL, Darden TA, Merz KM, Stanton RV, Cheng AL, Vincent JJ, Crowley M, Tsui V, Radmer RJ, Duan Y, Pitera J, Massova I, Seibel GL, Singh UC, Weiner PK, Kollman PA, Amber 6, University of California, San Francisco, (1999)

31. Jorgensen WL, Chandrasekhar J, Madura J, Impey RW, Klein ML (1983) J Chem Phys 79: 926-937

32. Ryckaert JP, Ciccotti G, Berendsen HJC (1997) J Comp Phys 23: 327-341

33. Berendsen HJC, Postma JPM, van Guensteren WF, DiNola A, Haak JR (1984) J Chem Phys 81: 3684-3690

34. Essmann U, Perera L, Berkowitz ML, Darden T, Lee H, Pedersen LG (1995) J Chem Phys 103: 8577-8593

35. Spakova N, Berger I, Sponer J (2001) J Am Chem Soc 123: 3295-3307

36. Humphrey W, Dalke A, Schulten K, "VMD – Visual Molecular Dynamics" (1996) J Mol Graph 14: 1, 33-38

37. Lu X-J, Shakked Z, Olson WK (2000) J Mol Biol 300: 819-840

38. Lavery R, Sklenar H, Curves 5.3 (http://apex.ibpc.fr/UPR9080/CurForm_bis.html)

39. Delbarre A, Delepierre M, Langlois d'Estaintot B, Igolen J, Roques BP (1987) Biopolymers 26: 1001-1033

40. Frøystein NÅ, Sletten E (1994) J Am Chem Soc 116: 3240-3250

41. Bostock-Smith CE, Harris SA, Laughton CA, Searle MS (2001) Nucl Acid Res 29: 3, 693-702

42. Kumar RA, Ikemoto N, Patel DJ (1997) J Mol Biol 265: 173-186

43. Chen H, Patel DJ (1995) J Mol Biol 246: 164-179

44. Wijmenga SS, Kruithof M, Hilbers CW (1997) J Biomol NMR 10: 337-350

45. Fouchet MH, Guittet E, Cognet JAH, Kozelka J, Gauthier C, Bret ML, Zimmermann K, Chottard JC (1997) J Biol Inorg Chem 2: 83-92

46. Marzilli LG, Saad JS, Kuklenyik Z, Keating KA, Xu Y (2001) 123: 2764-2770

47. Packer MJ, Dauncey MP, Hunter CA (2000) J Mol Biol 295: 71-83

48. Dickerson RE (1998) Nucl Acid Res 26: 8, 1906-1926

49. Bolshoy A, McNamara P, Harrington RE, Trifonov EN (1991) Proc Natl Acad Sci 88: 2312-2316

50. Hannon MJ, Meistermann I, Isaac CJ, Blomme C, Aldrich-Wright JR, Rodger A (2001) Chem Commun, 1078-1079

51. Meng EC, Shoichet BK, Kuntz ID (1992) J Comp Chem 13: 504-524

52. Merrit EA, Bacon DJ (1997) Meth Enzym 277: 505-524

Figure legends

Fig. 1. The molecular structure of the ligand (with numbering) and the tetracationic triple helical supramolecular cylinder $[Fe_2(C_{25}H_{20}N_4)_3]Cl_4$. A schematic route of synthesis is also shown.

Fig. 2. Imino ^1H NMR spectral region of $[d(GACGGCCGTC)_2]$ at 17°C with different $[Fe_2L_3]^{4+}$ to duplex ratios; (a) 0, (b) 0.25, (c) 0.5. The assignements of the imino signals from the complexed DNA are given in Table 1 based on NOESY spectra (data not shown).

Fig. 3. ^1H 2D- TOCSY spectrum of the $[d(GACGGCCGTC)_2]$ - $[Fe_2L_3]^{4+}$ sample showing the cytosine H5-H6 crosspeaks. The TOCSY spectrum was recorded with 80 ms mixing time at 25°C.

Fig. 4. Variations in chemical shifts between complexed and free DNA and the two strands of complexed DNA. Black bars are $\Delta\delta(H_I\text{-}H)$ and grey bars $\Delta\delta(H_{II}\text{-}H)$.

Fig. 5. ^1H 2D- NOESY spectrum of the $[d(GACGGCCGTC)_2]$ - $[Fe_2L_3]^{4+}$ adduct showing the sequential pathway for the aromatic - $H^{1'}/H^5$ region: (a) fre DNA, (b) the two strands in complexed DNA. The NOESY spectrum was recorded at 25 °C using a mixing time of 200 ms. The solvent is 90 % H_2O/ 10 D_2O. The sequential pathways for free DNA and the adduct are separated for clarity.

Fig. 6. Three snapshots taken from the trajectory and the average structure (1360-1500 ps). [d(GACGGCCGTC)$_2$] displays a remarkable flexibility during the course of the trajectory. The Fig. was generated with VMD [36] and Raster3D [52].

Fig. 7. Variation in DNA bending during the simulation cycles as measured by the distance between the centers of mass of the end base pairs in [d(G-A-C-G-G-C-C-G-T-C)$_2$].

Fig. 8. Plot of the RMS deviation between the equilibrated structure and the frames in the simulation trajectory.

Fig. 9. Variation in distances between the centre of mass in $[Fe_2L_3]^{4+}$ and the centre of mass of the two central base pairs G_5-C_{16} and C_6-G_{15} during the simulation cycles.

Fig. 10. Averaged structure over the last 200 ps from the 400 ps MD simulation including NOE restraints on the distances between S3 H7 and G4II H8, G5II H8 and C6II H6.

Fig. 11. Close-up of NOE contacts between S3 H7 and G4II H8, G5II H8 and C6II H6.

Fig. 12. A comparison of the structures from the unrestrained and NMR-restrained MD simulations. The structure from the NMR-restrained simulation is shown in thick lines. Hydrogens are omitted for clarity. The most notable differences in the two structures is the position of the cylinder and the displacements of the central base-

pairs. The total rms-deviation between the structures without hydrogens is 2.35 Å (calculated with VMD).

Fig. 13. Selection of helical parameters generated with 3DNA [37]. ▲= $[Fe_2L_3]^{4+}$/ DNA adduct, ●= Free DNA, ■= canonical B-DNA.

Fig. 14. Refined major groove widths generated with 3DNA [37].

Table 1. Chemical shifts (ppm) for free and complexed [d(GACGGCCGTC)$_2$]. The shifts are referred to the H_2O signal at 4.756 ppm at 25 °C. The chemical shift difference between the free and complexed DNA is presented in *italics*.

	H8/H6	H2/H5/CH3	H1'	H2'	H2''	H3'	H4'	H5'	H5''	NHB	NHF	H1/H3
G1	7.756		5.439	2.409	2.602	4.716	4.049	3.549	3.546			
A2	8.146	7.853	6.102	2.609	2.761	4.909	4.316	4.043	3.963			
C3	7.068	5.078	5.449	1.736	2.142	4.685	4.106	4.001	a	8.055	6.394	
$\Delta\delta_{(C3A-C3)}$	*0.046*	*0.063*	*-0.056*	*-0.013*	*-0.032*	*-0.018*	*-0.010*	*-0.011*	*n/a*	*-0.007*	*0.047*	
$\Delta\delta_{(C3B-C3)}$	*0.006*	*-0.001*	*0.011*	*0.045*	*0.095*	*0.034*	*-0.008*	*0.011*	*n/a*	*-0.003*	*n/a*	
G4	7.670		5.475	2.517	2.590	4.843	4.199	3.974	3.882			12.90
$\Delta\delta_{(G4A-G4)}$	*-0.106*		*-0.055*	*-0.141*	*-0.160*	*-0.053*	*-0.034*	*-0.041*	*-0.040*			*-0.05*
$\Delta\delta_{(G4B-G4)}$	*0.223*		*0.187*	*0.196*	*0.244*	*0.083*	*0.072*	*0.136*	*0.069*			*0.10*
G5	7.595		5.739	2.419	2.556	4.831	4.274	4.063	4.003			12.83
$\Delta\delta_{(G5A-G5)}$	*-0.310*		*0.203*	*-0.024*	*0.125*	*0.050*	*0.127*	*0.069*	*-0.008*			*0.03*
$\Delta\delta_{(G5B-G5)}$	*0.130*		*0.040*	*-0.331*	*-0.276*	*0.019*	*0.036*	*0.055*	*-0.003*			*0.03*
C6	7.177	5.101	5.783	1.909	2.312	4.679	4.056	3.971	3.918	7.950	6.179	
$\Delta\delta_{(C6A-C6)}$	*0.326*	*0.616*	*-0.316*	*-0.281*	*-0.213*	*0.126*	*0.531*	*-0.028*	*-0.249*	*0.214*	*0.813*	
$\Delta\delta_{(C6B-C6)}$	*0.518*	*0.602*	*0.536*	*0.210*	*0.210*	*0.149*	*0.065*	*-0.094*	*-0.160*	*0.197*	*0.804*	
C7	7.286	5.392	5.398	1.964	2.256	4.691	4.050	3.968	3.923	8.352	6.637	
$\Delta\delta_{(C7A-C7)}$	*-0.024*	*0.072*	*-0.009*	*0.038*	*0.013*	*-0.005*	*n/a*	*-0.171*	*-0.384*	*0.064*	*0.171*	
$\Delta\delta_{(C7B-C7)}$	*0.111*	*0.147*	*-0.022*	*0.102*	*0.035*	*0.053*	*n/a*	*0.057*	*-0.062*	*0.067*	*0.164*	
G8	7.795		5.871	2.521	2.651	4.843	4.243	3.989	3.921			12.70
$\Delta\delta_{(G8A-G8)}$	*0.022*		*0.022*	*0.000*	*0.000*	*0.000*	*0.053*	*0.000*	*0.000*			*0.04*
$\Delta\delta_{(G8B-G8)}$	*0.007*		*0.000*	*0.000*	*0.000*	*0.000*	*0.000*	*0.000*	*0.000*			*0.01*
T9	7.136	1.374	5.962	1.958	2.356	4.733	4.129	4.046	3.913			13.81
C10	7.451	5.575	6.103	2.114	2.114	4.432	4.042	3.864	a	8.097	6.982	

a) Not assigned due to overlapping signals.
n/a) Not applicable.

Table 2. Chemical shifts (ppm), at 25^{o}C, for $[Fe_2L_3]^{4+}$. The assignments for the free and complexed cylinder were obtained from a ROESY spectra in D_2O and NOESY spectra in H_2O, respectively. S1-S5 represents the five consistent sets of chemical shifts.

	H2	H3	H4	H5	H7	H10	H11	H13	H14	H15'	H15"
Free $[Fe_2L_3]^{4+}$	8.179	7.478	7.177	8.340	8.789	5.676	7.072	6.511	5.138	3.797	a
S1	8.188	7.471	7.094	8.320	8.735	5.106	6.247	5.339	4.062	2.696	2.362
S2	8.237	7.546	7.159	8.327	8.835	5.193	6.334	5.651	4.281	2.677	2.358
S3	8.224	7.484	7.092	8.393	8.897	5.476	6.530	5.805	4.945	2.618	1.361
S4	b	7.476	7.113	8.316	8.528	5.004	5.943	5.453	3.898	2.511	2.122
S5[c]	8.248	7.532	7.142	8.428	8.710	b	6.699	b	4.419	b	b

a) No dispersion between H15' and H15''.
b) Not assigned due to overlapping signals.
c) S5 do not display any NOE crosspeaks to DNA.

Table 3. NOE contacts between [d(GACGGCCGTC)$_2$] and $[Fe_2L_3]^{4+}$. The volumes of the crosspeaks are denoted with the letter s(strong), m(medium), w(weak) and vw(very weak). The volumes were measured relative to the H5-H6 (~2.5 Å) crosspeak in the cytosine for complexed DNA.

Helicate protons	Chemical shift(ppm)	Nucleic acid protons
S1 H7	8.735	G5A H1(m), G5A H8(w), C6A H5(m), C6A NHF(s)
S1 H11	6.247	G5A H1(m), G5A H8(m), C6A H5(s), C6A H6(m), C6A NHF(m), C6A NHB(m)
S1 H14	4.062	G5A H1(w)
S2 H2	8.237	G5A H1(vw), C6A H2(vw)', C6A H2''(w), C6A H5'(w), C6A H5''(w), C7A H5'(w), C7A H5''(vw)
S2 H3	7.546	C6A H5''(m), C7A H5''(w)
S2 H4	7.159	C6A H5''(w), C7A H5''(w)
S2 H5	8.327	G5A H1(w), C6A H2'(vw), C6A H2''(w), C6A H5''(w)
S2 H7	8.835	G5A H1(w), C6A H2'(w), C6A H2"(w), C6A H5(w), C6A H5''(w),C7A H5(vw), C7A H6(vw), C7A H5'(w), C7A H5''(w)
S2 H10	5.193	C6A H3'(vw), C6A H5''(vw)
S2 H11	6.334	G4A H8(vw), G5A H1(m), G5A H8(vw), C6A H2'(w), C6A H5''(w), C6A H5(m), C6A H6(m)
S2 H14	4.281	G4A H8(vw), G5A H1(m), G5A H8(w)
S3 H5	8.393	G5B H1(w)
S3 H7	8.897	G4B H8(vw), G5B H1(vw), G5B H8(vw), C6B H5(vw)
S3 H11	6.530	G5B H8(m), C6B H2'(vw), C6B H5(s), C6B H5''(vw)
S3 H15''	1.361	G5B H2'(vw), G5B H2''(w), G5B H8(m), C6B H3'(w), C6B H5(w), C6B H6(w)
S4 H5	8.316	C6B H2''(m), C6B H3'(m), C6B H5'(m),C6B H5(m), C6B H6(m), C7B H2''(w), C7B H5'(m), C7B H5(m), C7B H6(m)
S4 H7	8.528	G5B H1(m), C6B H3'(w), C6B H5''(vw), C6B H5(w), C6B H6(w), C7B H2''(vw), C7B H5'(m), C7B H6(vw)
S4 H10	5.004	G5B H8(w), C6B H5''(w), C6B H5(w), C6B H6(w), C7B H5(vw), C7B H6(w)
S4 H11	5.943	G5B H1(w), G5B H8(w), C6B H6(w)
S4 H14	3.898	G5B H1(m)

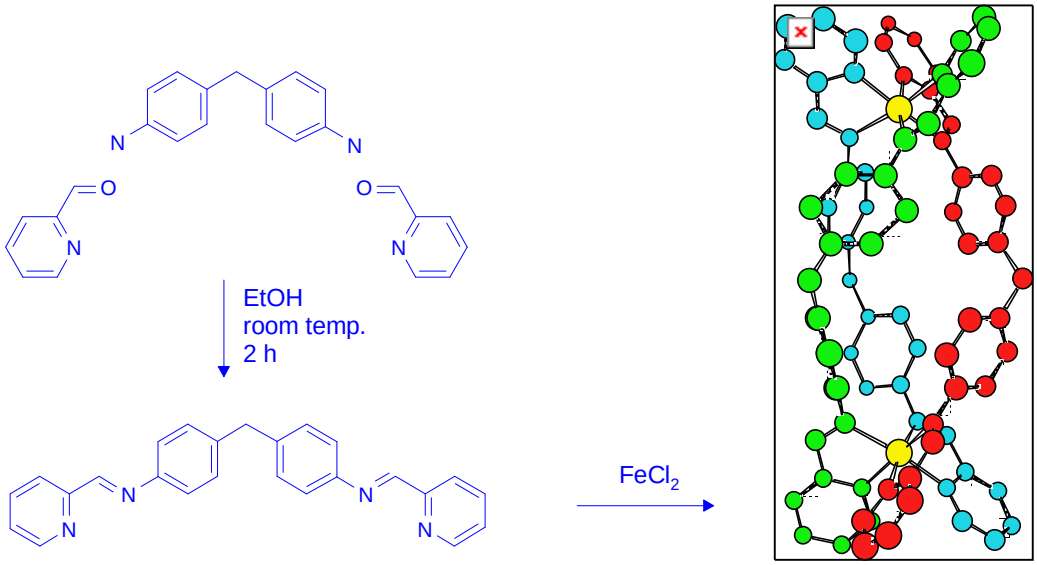

Figure 1. The molecular structure of the ligand (with numbering) and the tetracationic triple helical supramolecular cylinder $[Fe_2(C_{25}H_{20}N_4)_3]Cl_4$. A schematic route of synthesis is also shown.

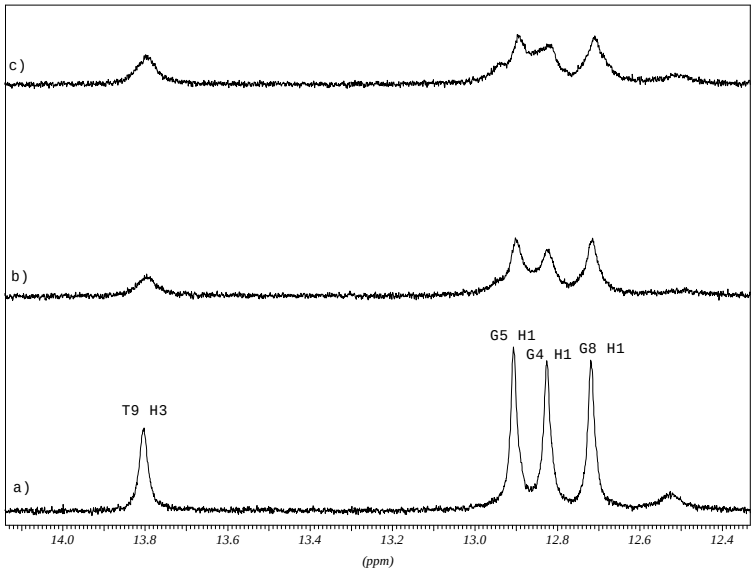

Figure 2. Imino ^1H NMR spectral region of [d(GACGGCCGTC)$_2$] at 17^{o}C at different $[Fe_2L_3]^{4+}$ to duplex ratios; (a) 0, (b) 0.25, (c) 0.5. The assignements of the imino signals from the complexed DNA are given in Table 1 based on NOESY spectra (not shown).

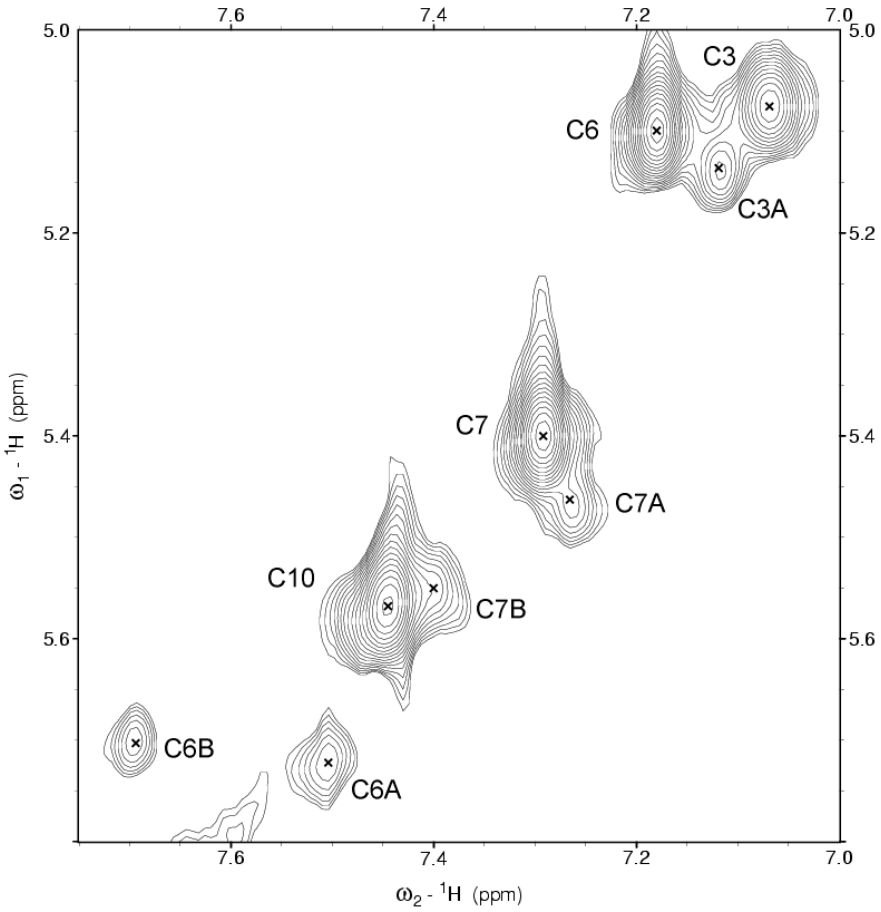

Figure 3. TOCSY spectrum showing the cytosine H5-H6 crosspeaks for free and complexed duplex recorded with 80 ms mixing time at 25 ºC.

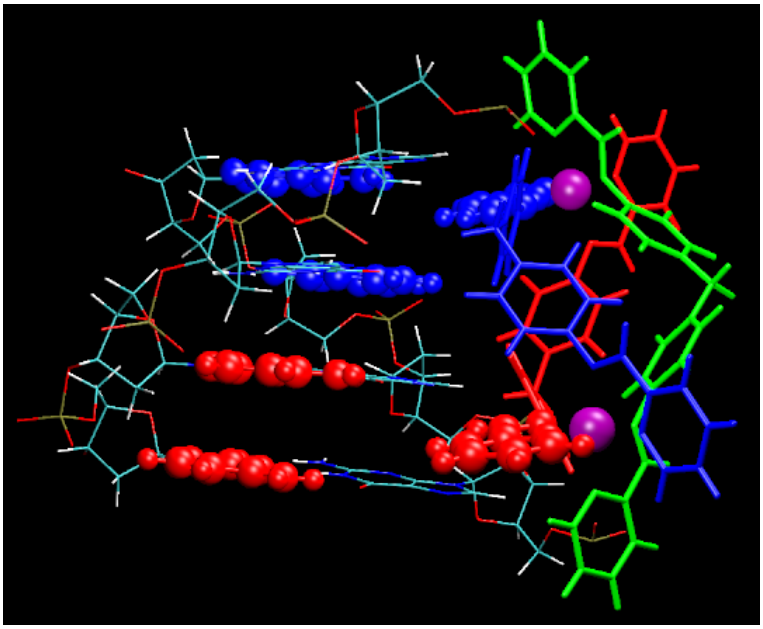

Figure 4. Results from the molecular docking calculation showing the remarkable fit of $[Fe_2L_3]^{4+}$ into the major groove of $[d(GACGGCCGTC)_2]$, here represented only with the central four base pair steps. Shown in red are the cytosines C6 and C7 and the pyridine ring facing the two bases. Shown in blue are the cytosines C16 and C17 and the corresponding pyridine ring. The figure was generated with VMD [38] and Raster3D [39].

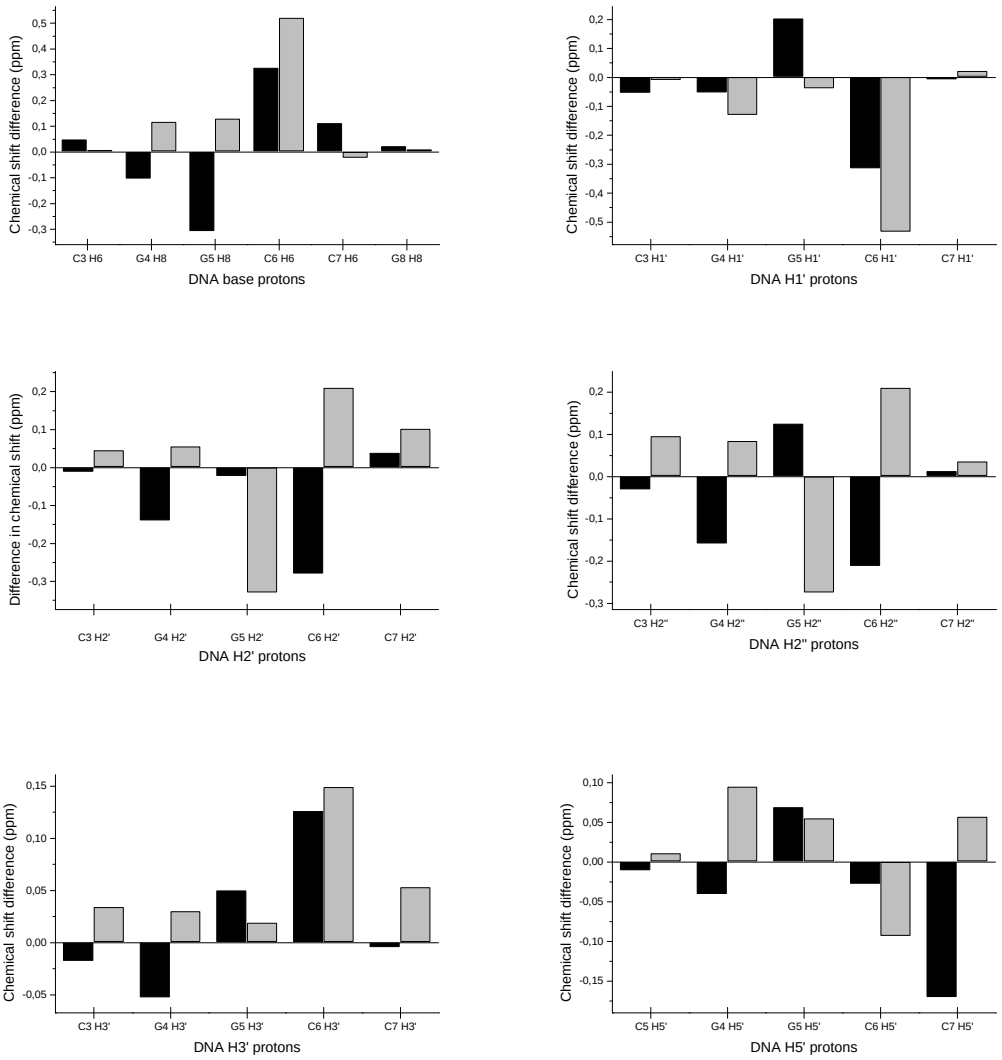

Figure 5. Variations in chemical shift between complexed and free DNA and the two strands of complexed DNA. Black bars are $\Delta\delta(H_A\text{-}H)$ and grey bars $\Delta\delta(H_B\text{-}H)$.

7a)

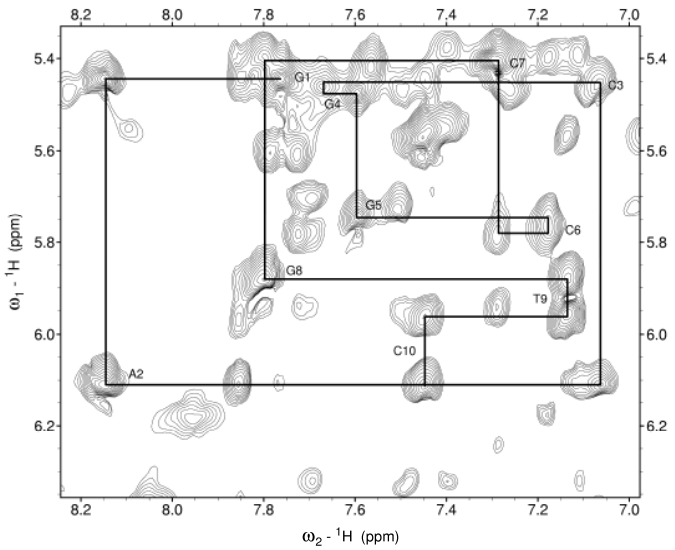

7b)

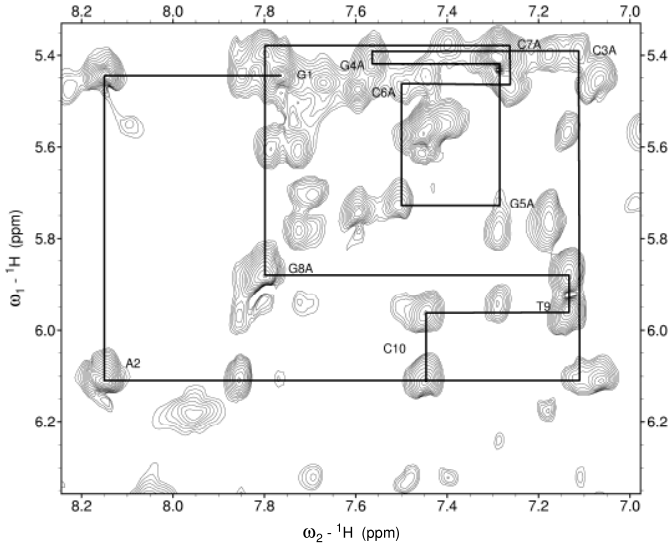

7c)

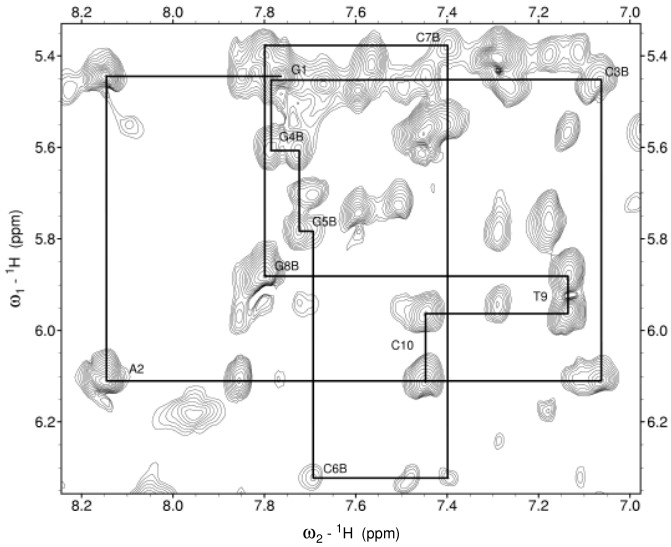

Figure 6. Proton 2D- NOESY spectrum of the $[d(GACGGCCGTC)_2]$ - $[Fe_2L_3]^{4+}$ adduct showing the sequential pathway for the aromatic - $H^{1'}/H^5$ region: (a) fre DNA, (b) and (c) the two strands in complexed DNA. The NOESY spectrum was recorded at 25 °C using a mixing time of 200 ms. The solvent is 90 % H_2O/ 10 D_2O. The three sequential pathways are separated for clearity.

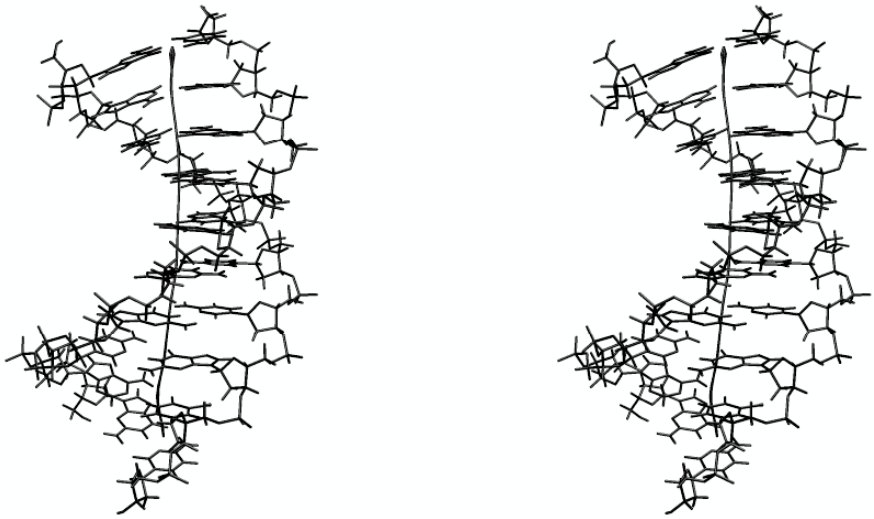

Figure 7. Stereo view of the average structure of free [d(GACGGCCGTC)$_2$]. The helical axis was included using Curves 5.3 [41].

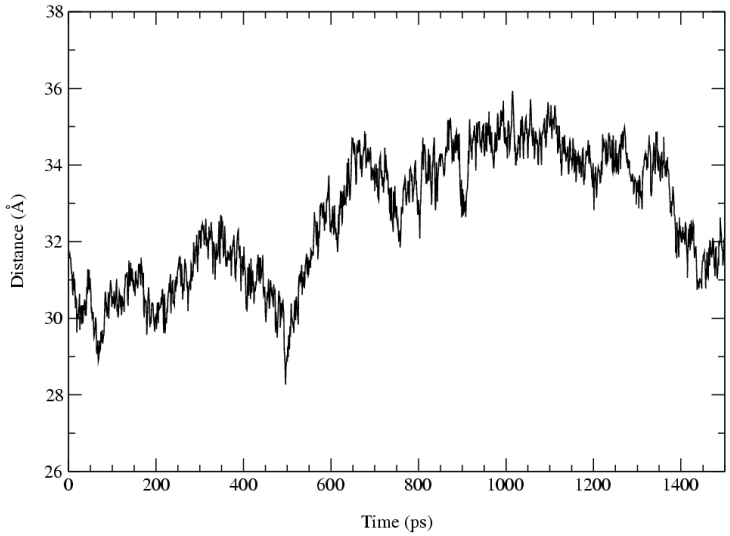

Figure 8. Variation in DNA bending during the simulation cycles as measured by the distance between the centers of mass of the end base pairs in [d(G-A-C-G-G-C-C-G-T-C)$_2$].

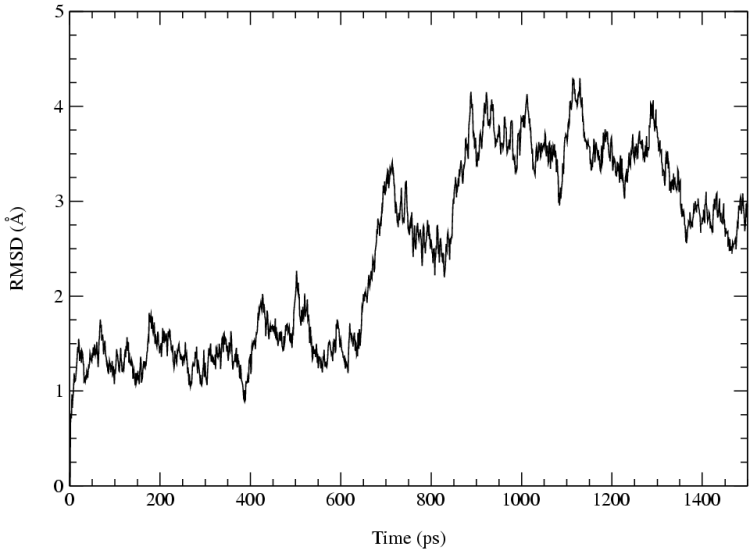

Figure 9. RMS deviation between the equilibrated structure and the frames in the simulation trajectory.

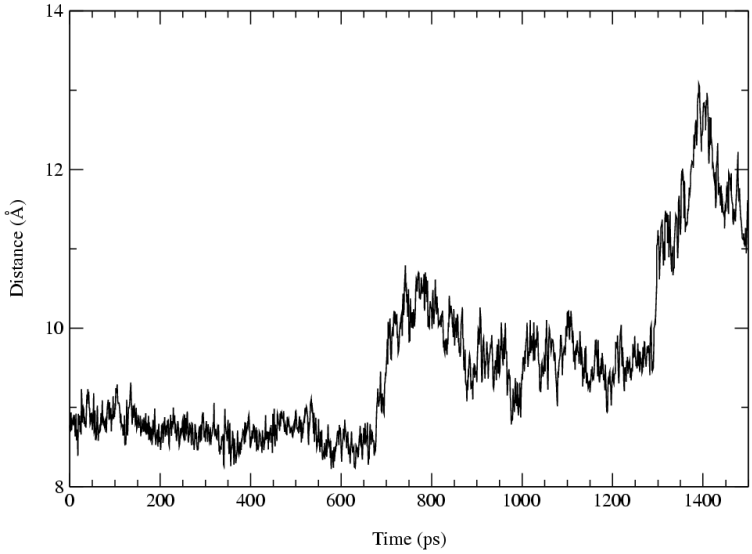

Figure 10. Variation in distances between the centre of mass in $[Fe_2L_3]^{4+}$ and the centre of mass of the two central base pairs G_5-C_{16} and C_6-G_{15} during the simulation cycles.

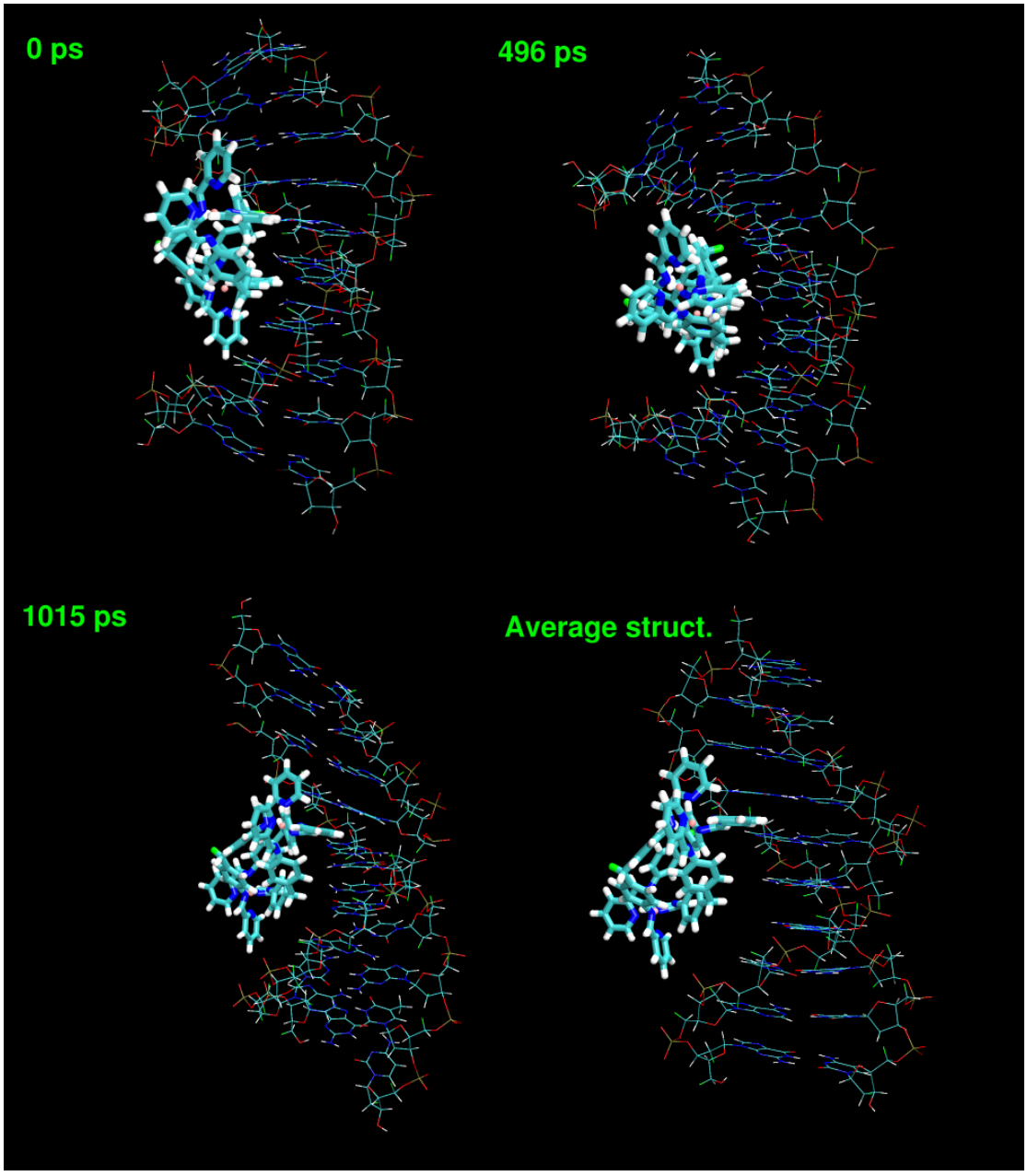

Figure 11. Three snapshots taken from the trajectory and the average structure (1360-1500 ps). [d(GACGGCCGTC)$_2$] displays a remarkable flexibility during the course of the trajectory.

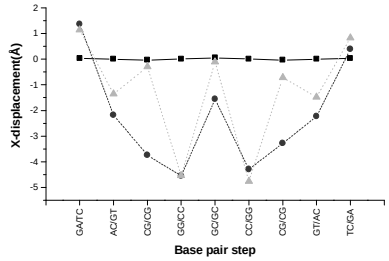
X-displacement(Å)
GA/TC
AC/GT
CG/CG
GG/CC
GC/GC
CC/GG
CG/CG
GT/AC
TC/GA
Base pair step

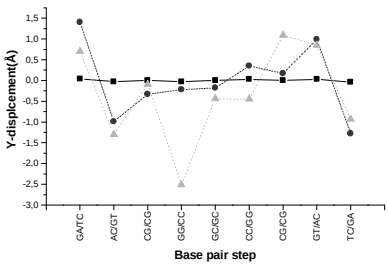
Y-displcement(Å)
GA/TC
AC/GT
CG/CG
GG/CC
GC/GC
CC/GG
CG/CG
GT/AC
TC/GA
Base pair step

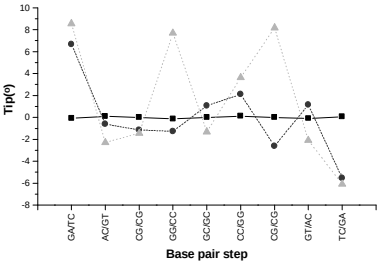
Tip(°)
GA/TC
AC/GT
CG/CG
GG/CC
GC/GC
CC/GG
CG/CG
GT/AC
TC/GA
Base pair step

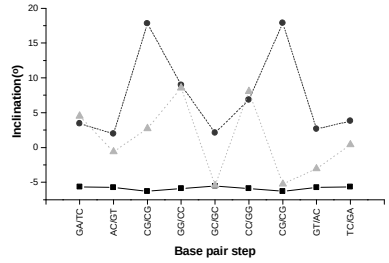
Inclination(°)
GA/TC
AC/GT
CG/CG
GG/CC
GC/GC
CC/GG
CG/CG
GT/AC
TC/GA
Base pair step

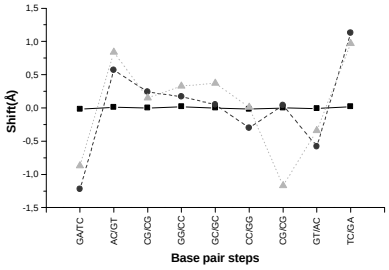
Shift(Å)
GA/TC
AC/GT
CG/CG
GG/CC
GC/GC
CC/GG
CG/CG
GT/AC
TC/GA
Base pair steps

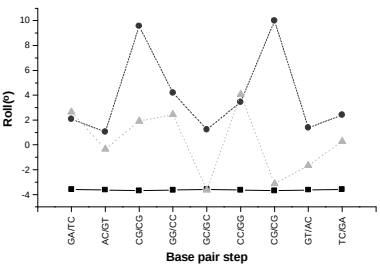
Roll(°)
GA/TC
AC/GT
CG/CG
GG/CC
GC/GC
CC/GG
CG/CG
GT/AC
TC/GA
Base pair step

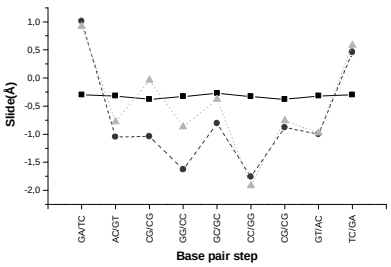
Slide(Å)
GA/TC
AC/GT
CG/CG
GG/CC
GC/GC
CC/GG
CG/CG
GT/AC
TC/GA
Base pair step

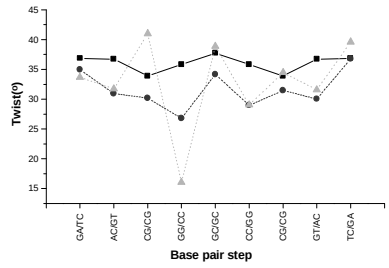
Twist(°)
GA/TC
AC/GT
CG/CG
GG/CC
GC/GC
CC/GG
CG/CG
GT/AC
TC/GA
Base pair step

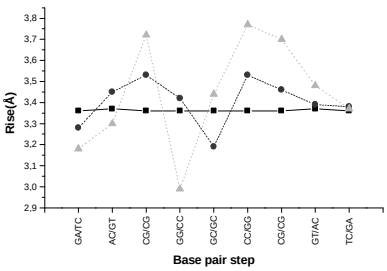
Rise(Å)
GA/TC
AC/GT
CG/CG
GG/CC
GC/GC
CC/GG
CG/CG
GT/AC
TC/GA
Base pair step

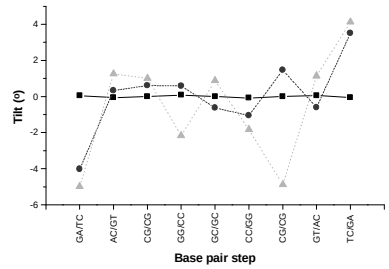
Tilt (°)
GA/TC
AC/GT
CG/CG
GG/CC
GC/GC
CC/GG
CG/CG
GT/AC
TC/GA
Base pair step

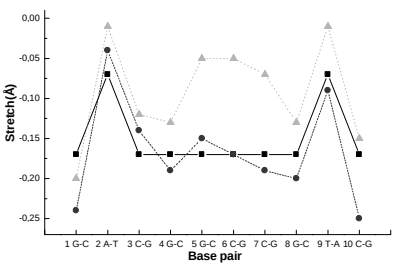
Stretch(Å)
1 G-C
2 A-T
3 C-G
4 G-C
5 G-C
6 C-G
7 C-G
8 G-C
9 T-A
10 C-G
Base pair

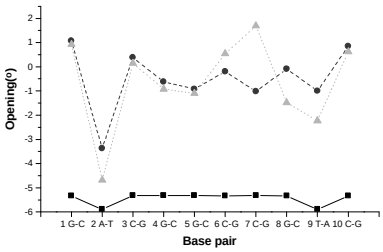
Opening(°)
1 G-C
2 A-T
3 C-G
4 G-C
5 G-C
6 C-G
7 C-G
8 G-C
9 T-A
10 C-G
Base pair

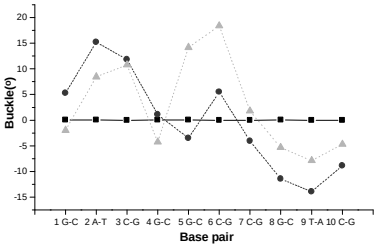
Buckle(°)
1 G-C
2 A-T
3 C-G
4 G-C
5 G-C
6 C-G
7 C-G
8 G-C
9 T-A
10 C-G
Base pair

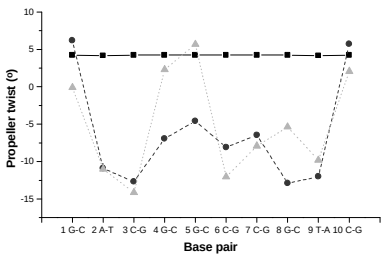
Propeller twist (°)
1 G-C
2 A-T
3 C-G
4 G-C
5 G-C
6 C-G
7 C-G
8 G-C
9 T-A
10 C-G
Base pair

Figure 12. Selection of helical parameters generated with X3DNA [39].
.....osv

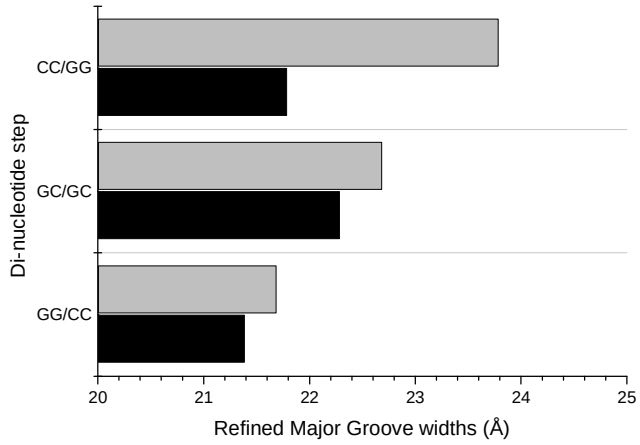

Figure 13. Refined major groove widths generated with X3DNA (39).

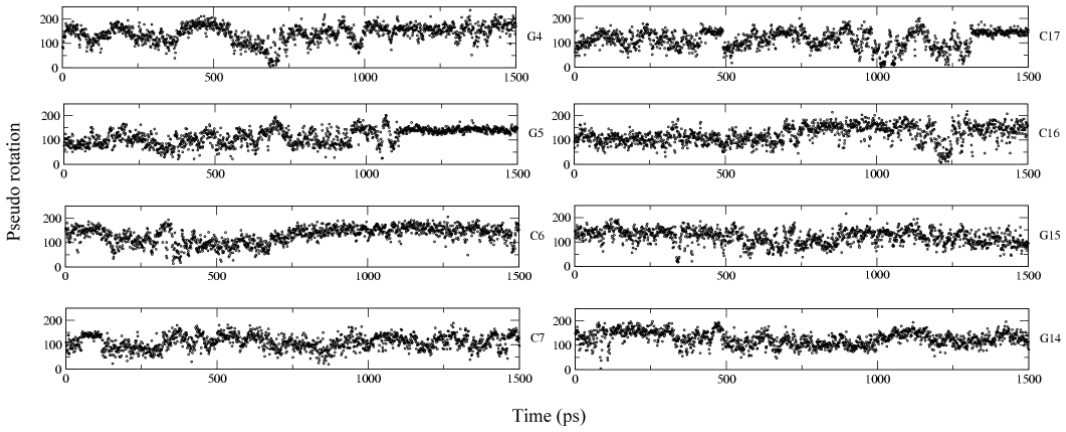

Figure 14. Plots of the pseudo rotation during the trajectory for the central tetranucleotide –GGCC-.